Transport of Copper Oxychloride-Based Fungicide Particles in Saturated Quartz Sand

PARADELO M.,[†] ŠIMŮNEK J.,[‡]
NOVOA-MUÑOZ J.C.,[†]
ARIAS-ESTEVEZ M.,[†] AND
J. EUGENIO LOPEZ-PERIAGO*,[†]

Soil Science Group, Department of Plant Biology and Soil Science, Faculty of Sciences, University of Vigo, E-32004 Ourense, Spain, and Department of Environmental Sciences, University of California Riverside, Riverside, California

Intensive use of copper-based fungicides in agriculture causes contamination of subsurface environment. While the transport of dissolved copper in porous media has been widely studied, transport mechanisms of particles of copper-based fungicides are poorly understood. This paper reports the results of tests involving the transport of colloid-size particles of a copper oxychloride-based fungicide (COF) in water-saturated quartz sand columns under varying electrochemical and hydrodynamic conditions. The effect of the ionic strength on colloid attachment and exclusion suggests that interactions of COF in water depend on the characteristics of the diffuse layer. Hydrodynamic shear influences the deposition of fungicide particles, indicating that attachment forces are weak. Particle deposition dynamics was well-fitted with the two-site kinetic attachment model, which reflects the heterogeneity of the quartz surface. Retention also occurs for unfavorable electrochemical conditions, which was attributed to stagnation zones arising from the physical and chemical heterogeneity of the quartz surface.

Introduction

Copper oxychloride-based fungicides (COFs) are widely used as foliar sprays against fungal diseases in a number of crops. Thus, there is a great likelihood that they may be released into the natural environment, especially soils. The accumulation of Cu in the soil from the use of COFs has been demonstrated in several studies (1–6). Current commercial formulations of copper fungicides use copper oxychloride powders with mean particle diameters of 1 μm. Off-target deposition and foliar wash-off induced by rainfall can facilitate the transfer of these fungicides into soils. Since copper oxychloride is poorly soluble (between 0.02 and 0.03 mmol Cu L^{-1} in equilibrium at 25 °C) in the typical pH range of rainwater (from 6 to 7), wash-off losses of particulate copper-oxychloride may be more substantial than the transport of dissolved forms of Cu, at least during heavy rain episodes. Laboratory studies have shown that losses of copper-based fungicides through wash-off occur mainly in the form of suspended particles (7).

While mechanisms governing the transport of dissolved forms of copper in porous media have been widely studied, the movement of copper-based particles is still poorly understood. Since various environmental factors affect mobility of soluble copper differently than the behavior of particulate forms, one can not predict travel distances of one substance from the knowledge of the other. In order to obtain better understanding of the mechanisms controlling the transport of particulate copper in saturated porous media, we examined the transport of colloidal COF in water-saturated quartz sand columns in terms of colloid deposition and colloid filtration theory.

Theory

The theory of colloid transport has been derived from the classical convection-dispersion equation (CDE) and the colloid attachment model. The attachment model assumes a first-order kinetic attachment of colloids, and an attachment coefficient that may decrease due to the filling of favorable attachment sites, or increase due to filter ripening. Straining represents the trapping of colloid particles when colloids are retained in pores that are smaller than some critical size. For an aqueous suspension of monodisperse particles flowing vertically through a packed column of granular collectors, the one-dimensional form of the CDE with two site kinetic attachment may be written (8):

$$\theta\frac{\partial c}{\partial t} = \frac{\partial}{\partial z}\theta\left(D\frac{\omega c}{\partial z} - Uc\right) - \rho_b\frac{\partial(s_{att1})}{\partial t} - \rho_b\frac{\partial(s_{att2})}{\partial t} \qquad (1)$$

where c is the colloid concentration in the aqueous phase [N L^{-3}], t [T] is time, z is the vertical spatial coordinate [L], θ is the volumetric water content [−], D is the hydrodynamic dispersion coefficient [L^2 T^{-1}], U is the average pore-water velocity [L T^{-1}], ρ_b is the bulk density of the porous matrix [M L^{-3}], and s_{att} [N M^{-1}] are concentrations of colloids attached to two different attachment sites, denoted by subscripts 1 and 2, respectively. The attachment rate to any of the two sites is given by

$$\rho_b\frac{\partial(s_{att})}{\partial t} = \theta k_{att}\Psi_{att}c - \rho_b k_{det}s_{att} \qquad (2)$$

where k_{att} and k_{det} are the first-order colloid attachment and detachment coefficients, respectively [T^{-1}], and Ψ_{att} is a dimensionless colloid attachment function [−]. Several functions examined in this work have been proposed in the literature to account for colloid deposition: Langmuirian (9), random sequential adsorption (RSA) (10), ripening, and depth dependent attachment (11).

The attachment coefficient, k_{att}, can be determined using the filtration theory (12), a quasi-empirical formulation that expresses the attachment coefficient in terms of the median grain diameter of the porous medium (often termed the collector), the pore-water velocity, and collector and collision (or sticking) efficiencies, accounting for colloid removal due to diffusion, interception, and gravitational sedimentation (12, 13). Here, we used the HYDRUS-1D program (8) to interpret the experimental particle breakthrough curves in light of the colloid attachment models and the colloid filtration theory.

Material and Methods

Copper Oxychloride. The copper oxychloride-based fungicide used in the tests (COF, manufactured by Industrias Químicas del Vallés S.A., Barcelona, Spain) contains 50% of

* Corresponding author phone: +34 988 387 070; fax: +34 988 387 001; e-mail: edelperi@uvigo.es.
† University of Vigo.
‡ University of California.

TABLE 1. Experimental Properties of the Fungicide

Cu content	g g^{-1}	0.535
mean particle size	μm	0.979
particle size distribution width	μm	0.272
particle density	g cm^{-3}	2.889

TABLE 2. Properties and Parameters of the Packed Quartz Sand Columns Used in the Fungicide Particle Deposition Tests

collector diameter (d_c)	cm	0.032
fluid density (ρ_f)	kg m^{-3}	10^3
fluid viscosity (μ)	kg m^{-1} s^{-1}	8.9×10^{-4}
temperature (T)	K	298
Hamaker constant (A)	J	1.0×10^{-20}
porosity (f)		0.41
column length (L)	cm	5
column diameter (L)	cm	1.5
Happel model parameter (A_s)		35.72

copper as a wetting powder (Table 1). The copper content of the commercial product was determined in quintuplicate using acid digestion with aqua-regia and hydrofluoric acid to the point of complete dissolution (*14*). The mineral composition as determined by an X-ray diffraction of crystalline powder on a Siemens D-5000 instrument revealed that the most abundant mineral phase is atacamite, and that there are traces of botallackite, wroewolfeite, and quartz; chemical elemental composition is reported in the Supporting Information.

A suspension containing 4 g of fungicide per L of distilled water (as recommended by the manufacturer) was prepared to determine pH. An aliquot of the suspension was filtered through a membrane of 0.45 μm pore size to determine the dissolved Cu. Another aliquot of the suspension (100 mL) was added, along with 5 mL 13.5 M HNO$_3$, to determine the soluble Cu in acid. Particulate Cu was calculated as the difference between soluble and total Cu. The average particle size diameter and ζ-potential of the fungicide powder in the aqueous suspensions were measured over the range 0.6 nm to 6 μm by dynamic light scattering on a Zetasizer Nano equipment from Malvern Instruments Ltd. (Malvern, UK). ζ-potentials were estimated from the electrophoretic mobility using Smoluchowski's approximation. Particle density was measured by pycnometry (*15*).

Quartz Sand. Quartz sand (SiO$_2$) was used as column packing material. Quartz grains were well sorted, with a grain diameter of 0.32 mm (Aldrich Chemical, Milwaukee, WI). The sand was thoroughly cleaned prior to use (*16*). Visual inspection by scanning electron microscopy confirmed that the sand grains were prolate spheroidal in shape. ζ-potential was measured in a near-micrometer size fraction, selected by sedimentation from a suspension of the ground sand sample.

Transport Tests. Clean quartz sand was wet-packed into adjustable chromatographic columns (Omnifit type, Sigma-Aldrich) 50 mm long and 15 mm in diameter, the top and bottom of which were covered with a nylon screen of 0.1 mm nylon mesh. The water content and the bulk density were determined by gravimetry in each test. Porosity was estimated from the water content, assuming that the water density at room temperature (20 °C) equals 0.9982 g cm^{-3} (*17*). Table 2 shows the most salient properties of the packed quartz sand columns used in the fungicide particle deposition tests. The longitudinal dispersivity of the column was estimated from transport tests using bromide as tracer.

The suspensions used in the column tests were prepared by mixing COF with distilled water or NaNO$_3$ solutions. Particles larger than 2.5 μm in equivalent diameter were removed by sedimentation. Copper concentration in the suspensions (measured after adding 13.5 M HNO$_3$, as indicated above) ranged from 93 to 130 mg L^{-1}. Particle density measurements were used in conjunction with nominal particle diameters to calculate the number of suspended particles. Fungicide suspensions were vigorously stirred while applied at the top end of the column via a Gilson minipuls III peristaltic pump.

Particle concentrations were measured by light absorption in a 80 μL flow-through cell from Hellma GmbH (Müllheim, Germany); measurements were made at a wavelength of 800 nm at 80 s intervals on a Jenway 6310 spectrophotometer. Effluent samples were also collected with a Gilson FC-203B fraction collector. The correlation between the light absorption of effluent and the total copper content in collected samples was used to calibrate the photometric readings. The total copper content in outflow samples was determined for fungicide suspensions as described above. Differences in mass balances of the eluted COF between replicate runs were less than 4%.

After the transport experiments have been finished, the sand was cut into slices 1 cm thick that were then digested with acid and dissolved Cu concentrations were then determined. The copper concentration in effluent fractions and sand extracts was measured on a Solaar M5 atomic absorption spectrophotometer from Thermofisher Scientific, Inc. (Waltham, MA), using an acetylene-air flame.

Experimental Plan. Column transport experiments of the fungicide in suspension (using NaNO$_3$ of 10^{-1}, 10^{-3}, 10^{-5} M and distilled water) were performed in order to obtain breakthrough curves, and to examine the influence of ionic strength on the attachment efficiency. The low range of electrolyte concentrations was chosen to represent heavy rainfall episodes when the soil solution is diluted. Ionic strength, pH, and ζ-potential of the fungicide particles were measured for each of the four suspensions. In addition, a test similar to that described in (*18*) was conducted in the following three steps, namely (1) deposition, similar as in the transport tests described above; (2) elution, by washing the quartz sand column containing the deposited fungicide with a fungicide-free solution with the same pH and ionic strength, and finally (3) further elution, using a solution with the substantially reduced ionic strength.

A third type of transport test, which involved suspending the fungicide in ionized water, and incorporated two different Darcy's velocities (0.57 cm min^{-1} and 2.83 cm min^{-1}), was performed in order to assess the influence of hydrodynamics on the fungicide deposition on sand grains.

Results and Discussion

The measured ζ-potential of the COF particles in the suspensions used in the deposition experiments (Table 3) became more negative as the ionic strength increased. Additional measurements in the range of electrolyte from 10^{-5} to 0.1 M (Figure 1) showed a minimum Zeta ζ-potential for electrolyte concentrations near 0.01 M. This behavior may be related to the so-called atypical behavior also reported in electrophoretic mobility experiments made with latex (*19*) and polystyrene spheres (*20*). This minimum could be a consequence of the relaxation (polarization of the electric double layer around the colloid during the ζ-potential measurement) that can cause mobility to increase as the surface true ζ-potential becomes more negative (*21*). Smoluchowski's approximation does not consider this relaxation. However, the maximum does not occur until the ζ-potential reaches an absolute value of 100 mV (*22*). Other researchers reported that anomalous behavior may also occur for high

TABLE 3. Properties of the Colloid Suspensions in Deionized (DW) Water Containing Variable Electrolyte Concentrations

NaNO3 concentration (mM)	pH	ζ-potential (mV)	copper in suspension (mg L^{-1})	fungicide concentration (mg L^{-1})	particle concentration, c_0 (particles L^{-1})
DW	6.1	−31	93	175	1.23×10^{11}
0.01	6.4	−35	130	243	1.71×10^{11}
1.0	6.3	−40	123	230	1.62×10^{11}
100.0	6.3	−47	93	174	1.23×10^{11}

electrolyte concentrations and surface charge densities when the counterion concentration in the immediate neighborhood of the surface is so large that the charge of colloids is overcompensated. This phenomenon is commonly referred to as overcharging (23). Multivalent counterions make a significant contribution to overcharging, and hence on the electrophoretic mobility of colloidal particles (24). In view of these studies, it is likely that Cu^{2+} dissolved from the copper oxychloride (from 0.062 to 0.075 mM, see SI Figure S1) can concentrate near the surfaces of fungicide particles, producing the so-called overcharging, the anomalous behavior observed here. A qualitative consequence of this phenomenon is that, due to small additions of $NaNO_3$, the presence of divalent (Cu^{2+}) rather than monovalent (Na^+) counterions intensifies counterion-particle attractions, and consequently, particle−particle attractions (25).

Given the electrochemical conditions imposed in the transport experiments, both the fungicide colloids and sand grains were negatively charged. Consequently, electrostatic repulsion between both types of particles may occur, at least for the lowest ionic strengths used in the deposition experiments in sand columns. However, the theoretical values of the Dejarguin−Landau−Verwey−Overbeek (DLVO) interaction energy profiles for colloids upon approach to collector surface predict the presence of an energy barrier (about 900 times greater than the thermal energy of colloids) against attachment at primary minima at the ionic strengths used here.

Influence of the Ionic Strength on the Fungicide Transport. The results of the colloid transport tests conducted at different ionic strengths are shown as breakthrough curves (BTC) in Figure 2. The relative colloid concentration in the effluent, C/C_0, increased rapidly at the start of each test. However, colloid attachment prevented the outflow concentrations from reaching the inflow concentration during each experiment. That means that colloid filtration still occurred despite of unfavorable electrochemical conditions for attachment predicted by the DLVO theory for ionic
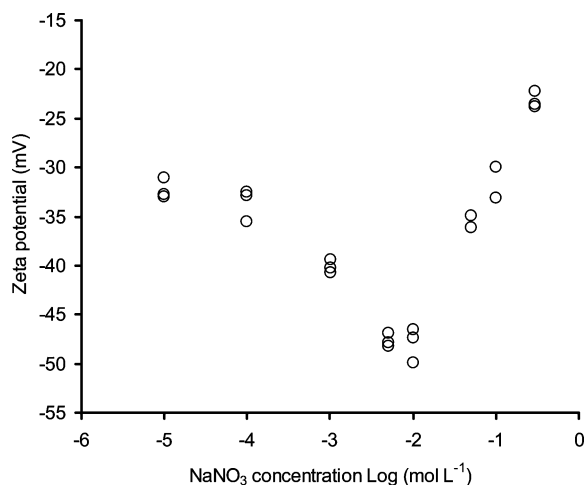
strengths smaller than 1 mM. The mass of particles retained in the columns for each of the experiments is shown in Table 4.
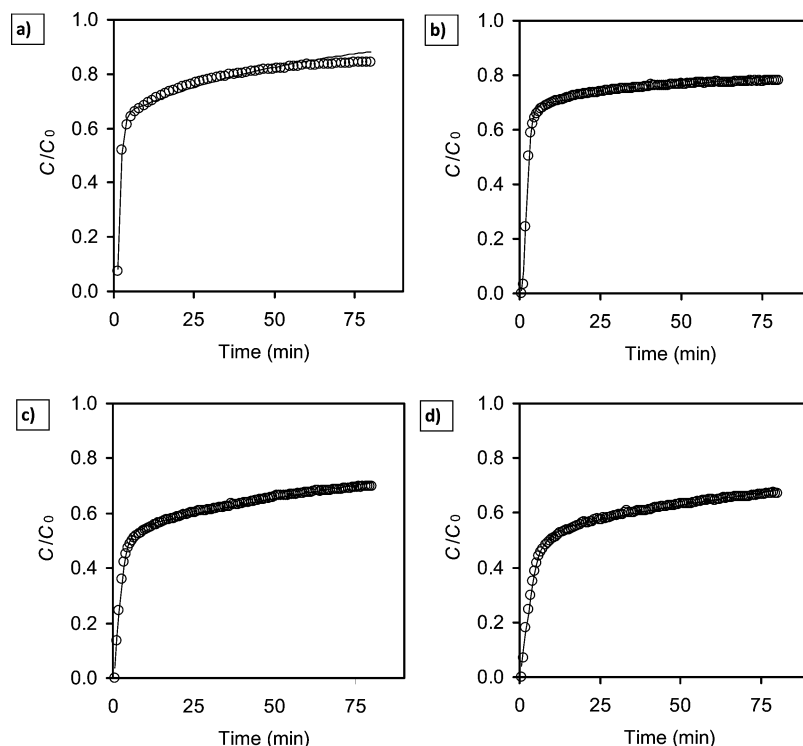
The experimental colloid BTCs (Figure 2a−d) were used to analyze particle deposition using the dispersivity length (0.01 cm) determined for the transport of Br$^-$. Several combinations of deposition models were tested. While the transport model with one site attachment was unable to reproduce the results, the two-site particle deposition model with blocking attachment functions offered good predictions for the experimental BTCs. Convergence and uniqueness of the parameters were tested by rerunning the program with different initial parameter estimates. Repeated runs resulted in the same final parameter set in all cases. This likely occurred because of the high data point density and low scattering of the experimental BTCs' data. The experimental concentration profiles were not exponential, indicating that the deposition of the COF could not be explained by the first-order deposition model without further modifications by various blocking functions (see SI Figure S2). Considering experimental particle concentration profiles together with the BTCs during parameter estimation did not significantly affect the final values of the fitted parameters. While the transport models that assumed either the ripening blocking function or the depth dependent colloid straining gave poor predictions of the BTCs, the transport model with an RSA attachment model for both attachment sites provided the best results. The RSA model was used to estimate the maximum attachment capacity, s_{max} and the attachment rate k_{att}. The RSA model defines an attachment function as follows:

$$\psi_{att} = 1 - 4a + 3.308a^2 + 1.4069a^3 \text{ for } s_{att} < 0.8s_{max} \tag{3}$$

$$\psi_{att} = \frac{(1 - bs_{att})^3}{2d_{50}^2 b^3} \text{ for } s_{att} \geq 0.8\, s_{max} \tag{4}$$

where $b = s_{max}^{-1}$ and $a = 0.546\, s_{att}/s_{max}$, in which s_{max} is the maximum solid phase concentration [M M^{-1}]. Fitted parameters of the two-site RSA model are presented in Table 4. Whereas one attachment type had a large capacity (from 1454 to 5760 mg Cu kg^{-1} sand) and slow kinetics (from 0.65 to 0.919 min^{-1}), the other had low capacity (from 60.2 to 112 mg Cu kg^{-1} sand) and was between 3 and 10 times faster (from 3.2 to 6.5 min^{-1}). The BTC obtained with distilled water (Figure 2a) shows that the deposition rate at later times was greater than predicted by the RSA, indicating a slow enhancement in deposition.

The maximum attachment capacity on the faster sites is close to the theoretical hard sphere jamming limit value of 0.546 (26). However, for the second type of the attachment site s_{max1} exceeds several times this value, suggesting that the surface area is larger than a sphere, or that multilayer deposition occurs. At ionic strengths smaller than 10^{-3} M, there is a increase in k_{att2} because the long-range of the double layer interactions favors increases in the attachment rate (22). Given the electrostatic repulsive forces, the long-range attractive interactions should occur at the secondary minimum for ionic strengths from 100 to 1 mM. Aggregation

FIGURE 1. Dependence of ζ-potential for copper-based fungicide particles on the solution ionic strength. Note a minimum of zeta potential at the ionic strength near 10^{-2} M.

FIGURE 2. Breakthrough curves for copper-based fungicide particles at different solution ionic strengths. Experimental conditions: Darcy fluid velocity $U = 2.83$ cm min^{-1}; collector diameter 0.032 cm; bed diameter 1.5 cm; column length 5 cm; temperature 25 °C. Symbols represent the experimental breakthrough curves and lines the two-site random sequential attachment model for (a) deionized water, and three different NaNO$_3$ concentrations of (b) 10^{-5} M; (c) 10^{-3} M; and (d) 10^{-1} M.

TABLE 4. Mass of Retained COF Particles and Fitting Parameters of the Two-Site Random Sequential Adsorption Model, As Estimated from the Particle Breakthrough Data Obtained in Saturated Packed Quartz Sand at Different Ionic Strengths (Standard Error of Fitting Parameters between Parentheses)

[a]I	[b]m	[c]m/m_0	[d]S_{max2}	[f]k_{att2}	[e]S_{max1}	[g]k_{att1}	[h]SSQ	[i]r^2
0.1	21	41	112 (2.2)	3.17 (0.106)	5060 (90.0)	0.91 (0.007)	0.005	0.995
0.001	18	38	91.8 (2.0)	2.87 (0.118)	5760 (83.8)	0.83 (0.005)	0.006	0.994
0.0001	14	27	102 (2.0)	6.11 (0.356)	4750 (159)	0.53 (0.005)	0.015	0.987
D.W.	12	23	60.2 (1.9)	6.89 (0.567)	1454 (49.2)	0.61 (0.008)	0.012	0.985

[a] Ionic stregth (mol L^{-1}). [b] Mass of particles retained in the column (mg). [c] Percentage retained. [d] Maximum capacity of attachment (mg Cu kg^{-1} sand). [e] Constant of attachment (min^{-1}). [f] Maximum capacity of attachment (mg Cu kg^{-1} sand). [g] Constant of attachment (min^{-1}). [h] Sum of squares of the residuals. [i] Squared Pearson's correlation coefficient.

between the COF particles prior to deposition may contribute to multi layer deposition, and therefore to the high S_{max1}. Also, the surface heterogeneity of the quartz grains may play a significant role. The low values of k_{att2}, in comparison with k_{att1}, indicate that the interactions in a multi layer deposition (i.e., aggregation between COF particles) may be of shorter range than between the COF and the clean quartz surface.

Tests involving variable NaNO$_3$ concentrations revealed that the attachment of the fungicide increased with increasing electrolyte concentrations, which we ascribed to an increasing collision efficiency. This behavior is in accordance with the standard Poisson–Boltzmann theory; as the ionic strength increased, diffuse double layers were compressed, and repulsive electrostatic double-layer forces between colloid particles diminished as a result. The discrepancy between ζ-potential measurements and colloid deposition experiments may reside in factors influencing electrophoretic mobility, such as polarization of the ion layer surrounding the colloid particles, and not from the attachment. Under chemically unfavorable attachment conditions (electrostatic repulsion), colloids would interact with the solid phase by virtue of the presence of secondary energy minima at separation distances greater than the location of the energy

barrier (27). However, attachment in the chemically unfavorable secondary minimum can significantly contribute to the retention of colloids in filtration experiments (28, 29).

Both heterogeneity and the influence of the electrolyte concentration suggest that the attachment exhibited in our experiments may occur in the secondary minimum. But, the depth of the secondary minimum is critical for its ability to create deposition. Figure 3 shows the representation of the total energy of interaction versus surface-to-surface separation distance profiles for quartz grains and COF particle sand calculated using the DVLO theory. It can be seen that using a typical value of the Hamaker constant for aqueous mineral dispersions of 10^{-20} J, the repulsive barrier lies in the range from 275 to 1564 K$_B$ T, whereas the depth of the secondary minimum from -73 to -15 K$_B$ T could explain colloid attachment for ionic strengths between 100 and 10 mM. Other factors that may have influenced attachment include the shape of the colloidal particles and non-DVLO forces. Heterogeneity of the surface of quartz sand, the presence of impurities, and heterogeneity in the shape and size of the fungicide particles can increase the retention well above what can be expected based on the DLVO theory (30).
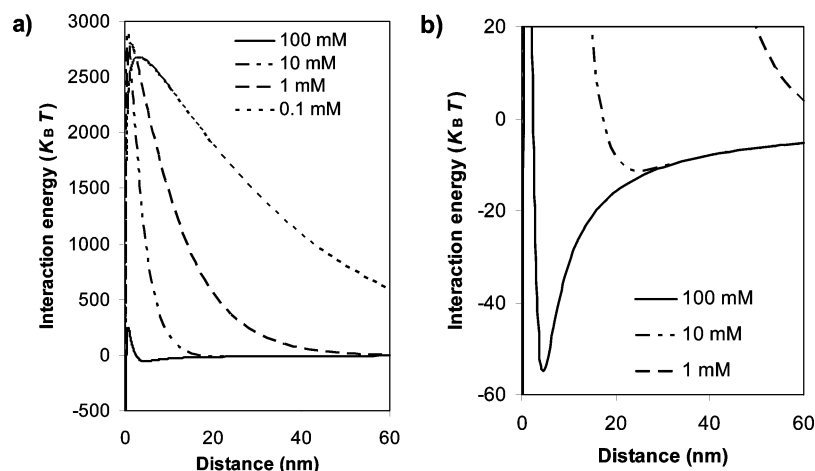
FIGURE 3. Representation of the total energy of interaction versus surface-to-surface separation distance profiles for quartz grain and colloid with sizes used in this work, suspended in aqueous electrolyte concentrations ranging from 0.1 to 100 mM. (a) Shows the repulsive maximum barrier that prevents attachment in the primary minimum; (b) The same data in enlarged beginning of the y-axis show the secondary minimum for each of the electrolyte concentration 1, 10, and 100 mM NaNO$_3$. The Hamaker constant for the quarz-water-COF system was $1.0 \ 10^{-20}$ J at 298 K.
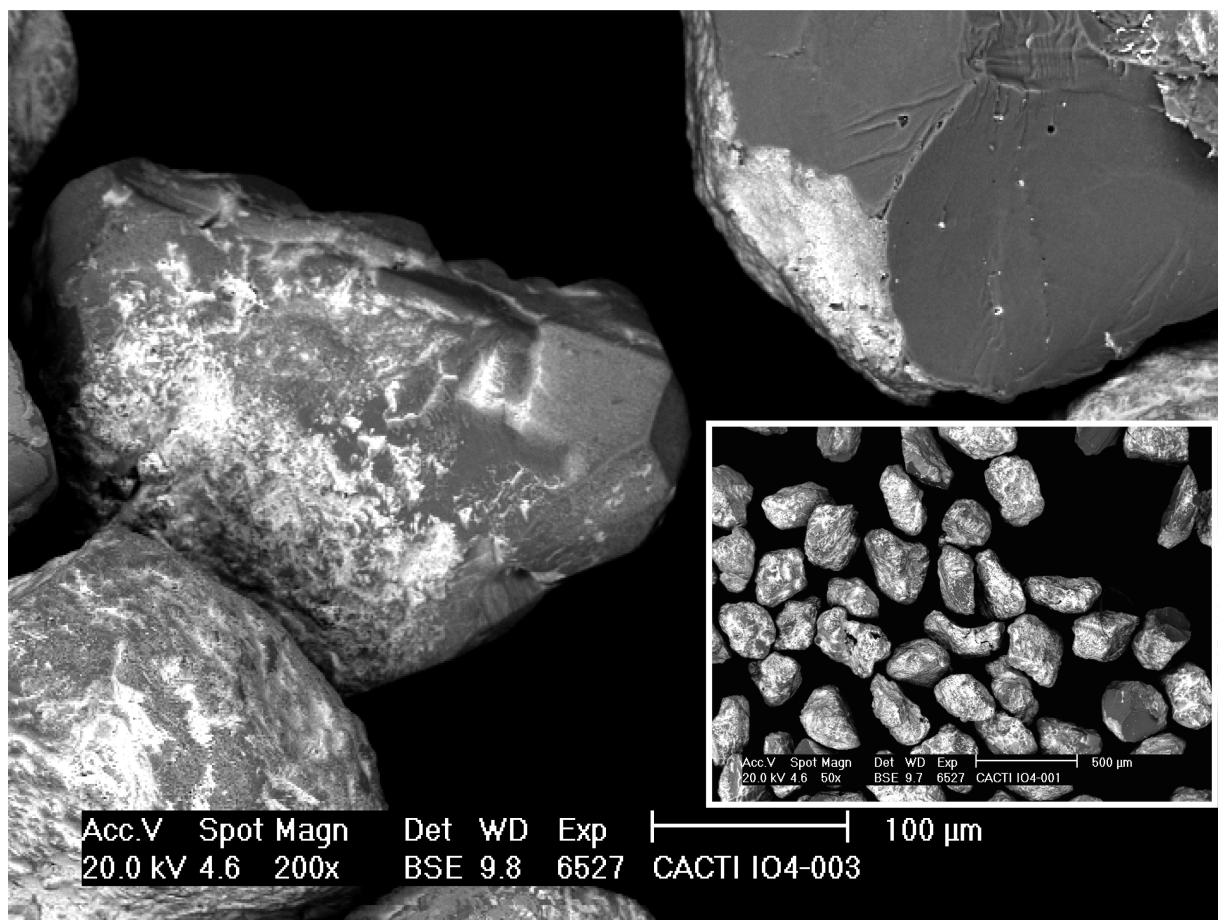

FIGURE 4. Scanning electron microphotographies of quartz sand grains covered with Fe obtained using the back scattering electron detector. The light areas correspond with a higher amount of sorbed Fe, whereas the darker areas are clean (less reactive) quartz surfaces (confirmed using the X-ray fluorescence microprobe). Note that the dark areas are flat, indicating a lower reactivity of the quartz crystal sides and minor local surface area, whereas light areas have a rougher surface and a greater local surface area.

The chemical and physical heterogeneity of the quartz sand surface was studied on a sample of coated iron-oxide grains (31) from the same sand batch. The surface analysis was carried out by scanning electron microphotography using backscattered electron detection and X-ray fluorescence probe. Since iron adsorbs preferentially to the negative surfaces, the amount of Fe adsorbed reveals the sites with more negative surface charge.

Figure 4 shows the chemically adsorbed iron patches (light patches) in the negatively charged sites, where dissociated silanol groups ($\equiv$Si—OH, pK_a ~3.5–6.9) occur at the pH ~6.3 used in the column experiments. Silanol groups are
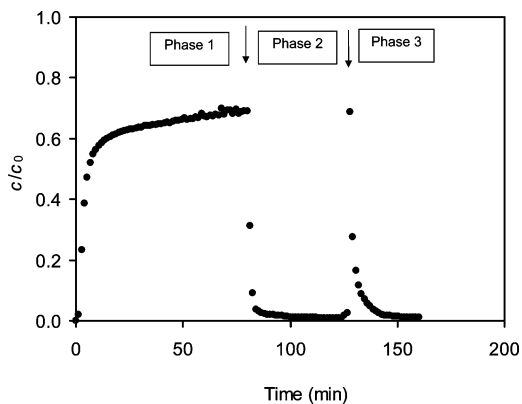
FIGURE 5. The three-phase breakthrough curve for fungicide particles. A suspension of fungicide particles was deposited at $s = 0.1$ M $NaNO_3$ in phase 1 (from 0 to 80 min), eluted with 0.1 M $NaNO_3$ in phase 2 (80 to 120 min), and further eluted with deionized water in phase 3 (from 120 to 160 min). Experimental conditions: water velocity $U = 2.83$ cm min^{-1}; collector diameter 0.032 cm; column diameter 1.5 cm; column length 5 cm; and temperature 25 °C.

located at imperfections in the crystal lattice; cracks and broken ends with more ruptured $-Si_2-O-Si-$ bonds per surface area. These patches also have higher roughness, which increases the local surface area available for attachment. The smooth crystal sides have less specific surface, which was revealed as dark patches with minor electrostatic repulsion (less negative charge). These surface properties agree with the two-site deposition model suggested by the colloid transport experiments. Therefore, the faster attachment sites with a low s_{max} correspond to low repulsion and smaller surface area, whereas the slower sites with higher repulsion have a high s_{max} due to larger surface area. The surface potential on the crystal sides would decrease below -30 mV, which is about the threshold potential of the repulsive barrier that the thermal Brownian energy can overcome, and this prevents particles from attaching in the primary minimum.

Mass balance shows that retention of 23% of particles still occurs for electrolyte concentrations smaller than 1 mM (i.e., without the secondary minimum), indicating that physical factors may also contribute to retention. A recent work shows that surface roughness of the collector may create zones of relative stagnation, in which pore space geometry and solution chemistry's coupled effects have a significant influence in colloid retention during transport (32).

Three-Phase Test. Based on the previous results, we assumed that the attachment of COF depends on the electrolyte concentration. In order to confirm this hypothesis, we ran a second test, during which we changed the electrolyte concentration within a single breakthrough (18).

The BTC for the three-phase experiment is shown in Figure 5. A suspension containing 1.4 10^{11} particles L^{-1} in 0.1 M $NaNO_3$ was applied during phase 1 to a column of packed quartz sand and about 25% of the particles were deposited in the column. Rinsing the column with 0.1 M $NaNO_3$ during phase 2 failed to elute a measurable quantity of deposited
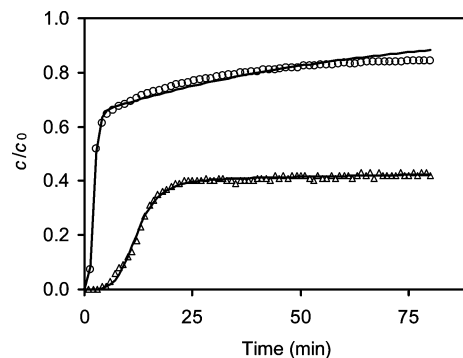
FIGURE 6. Breakthrough curves for copper-based fungicide particles showing the influence of the water velocity on particle attachment. Experimental conditions: collector diameter 0.032 cm; bed diameter 1.5 cm; bed depth 5 cm; temperature 25 °C. Symbols denote the results obtained at different water velocities $U = 2.83$ cm min^{-1} (circles) and 0.566 cm min^{-1} (triangles). Solid lines denote 2-sites RSA model.

fungicide. Rinsing of the column with deionized water during phase 3 released only 8.5% of the particles deposited during phase 1 and retained during phase 2. This result showed the influence of electrochemical conditions on the particle attachment. However, retention of particles in phase 3 supports the hypothesis that physical heterogeneity and porous space geometry may contribute to retention (32).

Hydrodynamic Effects. As can be seen from breakthrough curves obtained for different flow velocities (Figure 6), the maximum outflow concentrations decreased by a factor of 2 when flow velocity decreased five times. The fitted-parameters of the two-site kinetic attachment model shown in Table 5 indicate that slower flow results in an increase in s_{max1}. A decrease in attachment rates at both sites occurred when the inflow rate of the particles became limiting to retention.

The effect of hydrodynamics implies that the forces that keep the colloids attached in the s_{max2} are weak. The assumption of hydrodynamic influence on attachment is compatible with the weak forces at the secondary minimum, because increased shear stress forces would tend to pull attached colloids away (27). In addition, this behavior also suggests that increasing the flow rate tends to reduce stagnation zones, in which colloids can be retained.

To sum up, the results of depth-bed deposition tests with a copper oxychloride-based fungicide in water saturated quartz sand columns suggest the influence of the ionic strength and the hydrodynamic shear on the attachment rate. Attachment can occur in the weak secondary minimum for ionic strengths from 100 to 1 mM $NaNO_3$. However, retention in the absence of the secondary minimum (i.e., with ionic strength less than 1 mM) indicates that physical factors may also contribute to retention. Surface roughness of collector may create zones of relative stagnation, in which pore space geometry and solution chemistry's coupled effects have a significant influence on colloid retention during transport (32). This shows the importance of pore structure on colloid retention. Although attachment forces are weak,

TABLE 5. Fitting Parameters of the Two-Site Random Sequential Adsorption Model at Two Different Water Flow Velocities in Packed-Sand Columns

[a]U	[b]S_{max2}	[d]k_{att2}	[c]S_{max1}	[e]k_{attS1}	[f]SSQ	[g]r^2
2.83	60.2 (1.9)	6.89 (0.57)	1454 (49.2)	0.61 (0.01)	1.18×10^{-2}	0.985
0.57	55.3 (0.86)	1.56 (0.07)	9815 (1862)	0.26 (0.00)	4.36×10^{-3}	0.999

[a] Water flow velocity (cm min^{-1}). [b] Maximum capacity of attachment (mg Cu kg^{-1} sand). [c] Constant of attachment (min^{-1}). [d] Maximum capacity of attachment (mg Cu kg^{-1} sand). [e] Constant of attachment (min^{-1}). [f] Sum of squares of the residuals. [g] Squared Pearson's correlation coefficient.

the attachment of copper as oxychloride particles in quartz sand beds is larger than the maximum sorption capacity for dissolved copper in some acid soils (*33*). The environmental implications of these results lie in the fact that mobility of colloidal copper oxychloride-based fungicides is determined by characteristics of the diffuse layer, hydrodynamics and physicochemical heterogeneity of the porous media.

Acknowledgments

Supporting Information Available

Influence of electrolyte added ($NaNO_3$) in suspensions of copper-oxychloride fungicide on the activity of Cu^{2+}_{aq}, observed and predited profiles of concentration at the end of the breakthrough experiment using deionized water. This material is available free of charge via the Internet at http://pubs.acs.org.

Literature Cited

(1) Komárek, M.; Szákovaí, J.; Rohošková, M.; Javorská, H.; Chrastný, V.; Balík, J. Copper contamination of vineyard soils from small wine producers: A case study from the Czech Republic. *Geoderma* **2008**, *147*, 16–22.

(2) Pietrzak, U.; McPhail, D. C. Copper accumulation, distribution and fractionation in vineyard soils of Victoria, Australia. *Geoderma* **2004**, *122*, 151–166.

(3) Fernández-Calviño, D.; Nóvoa-Muñoz, J. C.; López-Periago, E.; Arias-Estévez, M. Changes in copper content and distribution in young, old and abandoned vineyard acid soils due to land use changes. *Land Degrad. Dev.* **2008**, *19*, 165–177.

(4) Rusjan, D.; Strlič, M.; Pucko, D.; Korošec-Koruza, Z. Copper accumulation regarding the soil characteristics in Sub-Mediterranean vineyards of Slovenia. *Geoderma* **2007**, *141*, 111–118.

(5) Moolenaar, S. W.; Beltrami, P. Heavy metal balances of an Italian soil as affected by sewage sludge and bordeaux mixture applications. *J. Environ. Qual.* **1998**, *27*, 828–835.

(6) Moolenaar, S. W.; Beltrami, P.; Ribolzi, O.; Valles, V.; Gomez, L.; Voltz, M. Speciation and origin of particulate copper in runoff water from a Mediterranean vineyard catchment. *Environ. Pollut.* **2002**, *27*, 835–271.

(7) Paradelo, M.; Arias-Estévez, M.; Nóvoa-Muñoz, J. C.; Pérez-Rodríguez, P.; Torrado-Agrasar, A.; López-Periago, J. E. Simulating washoff of Cu-based fungicide sprays by using a rotating shear device. *J. Agric. Food Chem.* **2008**, *56*, 5795–5800.

(8) Simunek, J.; Sejna, M.; Saito, H.; Sakai, M.; Van Genuchten, M. T. *The Hydrus-1D Software Package for Simulating the Movement of Water, Heat, and Multiple Solutes in Variably Saturated Media*, Version 4.0; Department of Environmental Sciences, University of California Riverside: Riverside, CA, 2008; Vol. 1, pp 315.

(9) Adamczyk, Z.; Siwek, B.; Zembala, M.; Belouschek, P. Kinetics of localized adsorption of colloid particles. *Adv. Colloid Interface Sci.* **1994**, *48*, 151–280.

(10) Johnson, P. R.; Elimelech, M. Dynamics of colloid deposition in porous media: Blocking based on random sequential adsorption. *Langmuir* **1995**, *11*, 801–812.

(11) Bradford, S. A.; Simunek, J.; Bettahar, M.; van Genuchten, M. T.; Yates, S. R. Modeling colloid attachment, straining, and exclusion in saturated porous media. *Environ. Sci. Technol.* **2003**, *37*, 2242–2250.

(12) Logan, B. E.; Jewett, D. G.; Arnold, R. G.; Bouwer, E. J.; O'Melia, C. R. Clarification of clean-bed filtration models. *J. Environ. Eng.* **1995**, *121*, 869.

(13) Rajagopalan, R.; Tien, C. Trajectory analysis of deep-bed filtration with the sphere-in-cell porous media model. *AIChE J.* **1976**, *22*, 523–533.

(14) Hossner, L. R. Dissolution for total element analysis. In *Methods of Soil Analysis Part 1-Chemical Methods*, 3rd ed.; Sparks, D. L., Ed.; American Society of Agronomy, Soil Science Society of America: Madison, WI, 1996; Vol. *2* pp 49–64.

(15) Blake, G. R. Hartge, K. H. Particle density. In *Methods of Soil Analysis. Part 1 Physical and Mineralogical Methods*, SSSA book Series no 5. 2nd ed.; Klute, A., Ed.; SAS, CSSA, and SSSA: Madison, WI, 1986; pp 377–382.

(16) Kuhnen, F.; Barmettler, K.; Bhattacharjee, S.; Elimelech, M.; Kretzschmar, R. Transport of iron oxide colloids in packed quartz sand media: Monolayer and multilayer deposition. *J. Colloid Interface Sci.* **2000**, *231*, 32–41.

(17) Lide, D. R. *CRC Handbook of Chemistry and Physics: A Ready-Reference Book of Chemical and Physical Data*; CRC Press: Boca Raton, FL, 2006; Vol. 1, pp 2608.

(18) Hahn, M. W.; O'Melia, C. R. Deposition and reentrainment of brownian particles in porous media under unfavorable chemical conditions: Some concepts and applications. *Environ. Sci. Technol.* **2004**, *38*, 210–220.

(19) Kobayashi, M. Electrophoretic mobility of latex spheres in the presence of divalent ions: experiments and modeling. *Colloid Polym. Sci.* **2008**, *286*, 935–940.

(20) Folkersma, R.; van Diemen, Alois J. G.; Stein, H. N. Electrophoretic properties of polystyrene spheres. *Langmuir* **1998**, *14*, 5973–5976.

(21) O'Brien, R. W.; White, L. R. Electrophoretic mobility of a spherical colloidal particle. *J. Chem. Soc. Faraday Trans.* **1978**, *74*, 1607–1626.

(22) Elimelech, M.; Gregory, J.; Jia, X.; Williams, R. A. *Particle Deposition and Aggregation: Measurement, Modelling, And Simulation*; Butterworth-Heinemann: Oxford, UK, 1995; p 433.

(23) Quesada-Pérez, M.; González-Tovar, E.; Martín-Molina, A.; Lozada-Cassou, M.; Hidalgo-Álvarez, R. Overcharging in colloids: Beyond the Poisson-Boltzmann approach. *Chem. Phys. Chem.* **2003**, *4*, 234–248.

(24) Quesada-Pérez, M.; González-Tovar, E.; Martín-Molina, A.; Lozada-Cassou, M.; Hidalgo-Álvarez, R. Ion size correlations and charge reversal in real colloids. *Colloids Surf., A* **2005**, *267*, 24–30.

(25) McBride, M. B.; Baveye, P. Diffuse double-layer models, long-range forces, and ordering in clay colloids. *Soil Sci. Soc. Am. J.* **2002**, *66*, 1207–1217.

(26) Hinrichsen, E. L.; Feder, J.; Jøssang, T. Geometry of random sequential adsorption. *J. Stat. Phys.* **1986**, *44*, 793–827.

(27) Torkzaban, S.; Bradford, S. A.; Walker, S. L. Resolving the coupled effects of hydrodynamics and DLVO forces on colloid attachment in porous media. *Langmuir* **2007**, *23*, 9652–9660.

(28) Redman, J. A.; Walker, S. L.; Elimelech, M. Bacterial adhesion and transport in porous media: Role of the secondary energy minimum. *Environ. Sci. Technol.* **2004**, *38*, 1777–1785.

(29) Tufenkji, N.; Elimelech, M. Breakdown of colloid filtration theory: Role of the secondary energy minimum and surface charge heterogeneities. *Langmuir* **2005**, *21*, 841–852.

(30) Shani, C.; Weisbrod, N.; Yakirevich, A. Colloid transport through saturated sand columns: Influence of physical and chemical surface properties on deposition. *Colloid. Surf., A* **2008**, *316*, 142–150.

(31) Johnson, P. R.; Sun, N.; Elimelech, M. Colloid transport in geochemically heterogeneous porous media: Modeling and measurements. *Environ. Sci. Technol.* **1996**, *30*, 3284–3293.

(32) Torkzaban, S.; Tazehkand, S. S.; Walker, S. L.; Bradford, S. A. Transport and fate of bacteria in porous media: Coupled effects of chemical conditions and pore space geometry. *Water Resour. Res.* **2008**, *44*, W04403.

(33) López-Periago, J. E.; Arias-Estévez, M.; Nóvoa-Muñoz, J. C.; Fernández-Calviño, D.; Soto, B.; Pérez-Novo, C.; Simal-Gándara, J. Copper retention kinetics in acid soils. *Soil Sci. Soc. Am. J.* **2008**, *72*, 63–72.

ES901650G